Geomechanics and Engineering, *Vol. 41, No. 3 (2025) 365-380*
https://doi.org/10.12989/gae.2025.41.3.365

Numerical analyses for the bearing behavior and uplift potential of single pile in water-sensitive expansive soils

Xilin Lü[1,2], Yishun Zhong[1,2], Dawei Xue*[2], Zheng Su[1,2] and Huanhuan Du[3]

[1]*Department of Geotechnical Engineering, Tongji University, Shanghai 200092, China*
[2]*Key Laboratory of Geotechnical and Underground Engineering of Ministry of Education, Tongji University, Shanghai 200092, China*
[3]*College of Architecture and Energy engineering, Wenzhou University of Technology, Wenzhou, 325035, China*

(*Received May 22, 2024, Revised February 21, 2025, Accepted March 11, 2025*)

Abstract. The swelling/shrinkage behavior of expansive soils in relation to water content may pose considerable threats to the infrastructures above them. While piles are commonly used to address this issue, the performance of pile-soil systems is usually elusive. In this context, the paper numerically studies the bearing behavior and uplift potential of a single pile in expansive soils. To this end, the stress-strain responses and shear strength variation of expansive soil specimens under different water contents are experimentally investigated through a series of consolidated undrained (CU) triaxial tests. Based on the dataset, three-dimensional (3D) finite element analyses of a single pile in expansive soils are conducted using the thermo-mechanical module of ABAQUS. This approach utilizes the association between water-induced soil swelling/shrinkage behavior and that caused by temperature changes. The results reveal that as the water content within the effective depth increases, the ultimate bearing capacity of the pile initially rises and then declines, due to the competing mechanism between soil strength reduction induced by water infiltration and the upward soil-to-pile friction provided by soil swelling effects. Such a competing mechanism is shown to play a non-negligible role in affecting the interplay between the pile uplift potential and water content. In addition, the uplift potential is also influenced by the variation in pile self-weight due to the change of pile length or diameter.

Keywords: bearing behavior; expansive soils; finite element modeling; pile; soil swelling

1. Introduction

The strength and volume of an expansive soil sample, usually composed of montmorillonite, illite, and hydrophilic minerals, can undergo significant changes with variations in water content (Lavanya and Kumar 2021). Expansive soils, in fact, exhibit swelling when exposed to certain amounts of water and shrinkage as the water evaporates. The former corresponds to strength reduction while the latter is related to strength enhancement. This undesired water-sensitive deformation property can pose considerable threats to the infrastructures built upon expansive soil foundations (Aziz *et al*. 2015, Mohanty *et al*. 2017, Jain *et al*. 2020, Wei *et al*. 2022, Abden *et al*. 2024).

In recent decades, advancements in the understanding of expansive soils, particularly regarding their swelling behavior, have been achieved, thanks to numerous investigations. For example, through laboratory experiments, Al-Yaqoub *et al*. (2017) observed that significant swelling of expansive soils is promoted when the degree of saturation exceeds 80%. The swelling rate of expansive soils can be affected by both the wetting process and surcharge pressure. The experimental study reported by Yan and Wu (2009) has revealed negative exponential relations between swelling pressure and initial water content. Besides, they found that swelling deformation has a negative linear correlation with initial water content and a negative exponential relation to external pressure. From an engineering perspective, it is essential to propose suitable strength descriptions considering the effects of water content for expansive soils (Iizuka *et al*. 2019). The unsaturated shear strength criterion proposed by Fredlund *et al*. (1978) involves two independent stress variables, namely net normal stress (σ-u_a) and matric suction (u_a-u_w). The effects of osmotic suction from salt dissolution on the strength characteristics of expansive soils have also been considered (Bai and Liu 2012). The sum of osmotic suction and matric suction is known as the total suction, a critical factor affecting the deformation responses of expansive soils. Pronounced suction effects may lead to a nonlinear increase in shear strength and dilatancy of expansive soils (Zhan and Ng 2006, Ye *et al*. 2010, Bai and Liu 2012, Zhang *et al*. 2020). The shear strength of expansive soils is also reported to increase with increasing dry density (Xiao *et al*. 2018, Zhang *et al*. 2020) but decreases with the water content (Miao *et al*. 2002, Ye *et al*. 2010). In the context of Mohr-Coulomb strength criteria, the shear strength of expansive soil can be simply described by two parameters, i.e., cohesion and friction angle. Bai and Liu (2012) have found that the cohesion of expansive soils decreases exponentially with water content. Chowdhury and Azam (2016), however, reported that the cohesion initially increases and then decreases as water content increases. This phenomenon may be explained by the mobilization of

*Corresponding author, Ph.D.
E-mail: dawei.xue93@gmail.com

ISSN: 2005-307X (Print), 2092-6219 (Online)

cohesion caused by suction effects at relatively low water content, and a reduction of cohesion due to suction dissipation with a further increase in water content. The experimental study by Chowdhury and Azam (2016) also revealed that the friction angle keeps decreasing with the water content due to the water-induced strong lubrication between soil particles. When a certain water content is reached, however, the friction angle may remain constant with a further increase in water content (Bai and Liu 2012).

Pile-supported foundations have been widely used to reduce the differential settlement of soil and resist loads transferred from the superstructures (Fattah *et al*. 2013, Khanmohammadi and Fakharian 2018, Bhaduri and Choudhury 2020), as well as to prevent undesired deformation of geosystems involving expansive soils (Nelson *et al*. 2012, Burke *et al*. 2022, Alnmr *et al*. 2023). To date, some research works have been implemented to explore the performance of piles in expansive soils. The load transfer mechanism of piles in expansive soils has been studied by Fan *et al*. (2007). Xiao *et al*. (2011) discovered that increasing pile length can diminish pile uplift yet can lead to non-negligible tensile stress along the pile. Additionally, the axial tensile stress and pile uplift movements increase with the duration of water exposure to soil samples. Moreover, through physical model tests, Hou *et al*. (2021) illustrated that the relative displacement between pile and soil increases significantly over water immersion time but eventually reaches a stable value. The axial force and side friction initially increase with the duration of water immersion and slightly decrease after reaching peak values, as observed by Liu *et al*. (2022). Liu and Vanapalli (2017) have carried out experiments on the behavior of soil-pile systems under the effect of lateral soil swelling. The expansive soil body can be divided into an active zone, in which external water invasion triggers water content variation and soil swelling, and a stable zone where water content and soil swelling behavior are insensitive to external fluid input. In fact, after water infiltration, upward friction applied by soils to the pile can be generated in the active zone, while in the stable zone, this friction reverses its direction. The upward friction can be estimated by considering the contributions provided by cohesion, matric suction, and the normal stress between pile and soil, as suggested by Liu and Vanapalli (2017). Liu and Vanapalli (2021) further showed that water infiltration mobilizes the lateral swelling pressure, potentially increasing pile-soil friction, and leading to pile uplift displacement. On the other hand, the increasing water content may cause the reduction of matric suction and interface shear strength, diminishing pile-soil friction and thus reducing the potential for pile uplift (Liu and Vanapalli 2019). In fact, identifying the interaction between piles and expansive soils with varying water content is attractive but complicated. Recent studies have advanced the understanding of pile behavior in expansive soils by developing constitutive models and simulating water infiltration effects (Wu and Vanapalli 2022), integrating unsaturated soil properties and effective stress in finite element analysis (Alnmr *et al*. 2024), and coupling subsurface flow, soil deformation, and hygroscopic swelling in numerical simulations (Awadalseed *et al*. 2024). Nevertheless, these reported simulations are time-consuming due to the necessity of incorporating water-sensitive soil strength and the complexity of modeling swelling/shrinkage soil behavior in full-field simulations. Besides, research considering the influence of both water content reduction and pile dimensions remains limited.

In response to these aspects, the work reported in this paper investigates the bearing behavior and uplift potential of a single pile in expansive soils using a data-driven numerical simulation strategy where the soil swelling/shrinkage behavior is properly simulated. Specifically, the water content effects on soil shear strength parameters are assessed through a series of consolidated undrained (CU) triaxial tests and are considered in the established three-dimensional (3D) finite element numerical model for a pile-soil system. In addition, the link of water-induced soil swelling/shrinkage behavior to that caused by temperature changes is used, thus benefiting the modeling of water-sensitive swelling/shrinkage soil behavior in full-field simulations. This approach is implemented in the finite element platform ABAQUS, via the thermo-mechanical module. The bearing behavior and uplift potential of the pile in relation to pile length, diameter, and water content are finally analyzed and discussed.

2. Consolidated undrained (CU) triaxial tests

This work focuses on the numerical investigation of the bearing behavior and uplift potential of single pile within water-sensitive expansive soils using the finite element (FE) method. The Mohr-Coulomb model is selected due to its simplicity and ease of calibration. To achieve this goal, a series of consolidated undrained (CU) triaxial tests are performed, with the aim of obtaining key soil parameters (i.e., elastic modulus, cohesion, and friction angle) and their correlations with water content.

2.1 Specimen preparation

The original expansive soils used in this study are sourced from Nanyang City, Henan Province, China, as depicted in Fig. 1(a). These in situ soils display an average natural water content of 22.47%, a natural density of 2.07 g/cm³, a plastic limit (PL) of 18.2%, a liquid limit (LL) of 28.5%, and a free swelling ratio of 57%. Based on these properties, the soils are classified as weak expansive soils (GB 50112, 2013).

For the triaxial tests, specimens are prepared at five different initial water contents: 7.65%, 13.78%, 19.90%, 26.03%, and 31.00%. The specimen preparation involves the following steps: (i) the in situ soils are crushed and sieved using 2.0 mm openings, followed by oven drying for 8 hours at 105°C; (ii) the dried soils are thoroughly mixed with water to achieve the desired initial water contents, and then stored in a sealed wet-keeping container for at least 48 hours to ensure well-proportioned water distribution in the samples, as shown in Fig. 1(b); and (iii) the soil samples are compacted in a cylindrical steel mold using a compacting instrument, resulting in triaxial test specimens with a

(a) Expansive soils collected from the field

(b) Mixture of dried soils and water

(c) Prepared specimen for triaxial tests

Fig. 1 Soil sampling and specimen preparation

(a) The GDS stress path triaxial system

(b) The installation of specimens

Fig. 2 Configuration of consolidated undrained triaxial tests

diameter of 39.1 mm and a height of 80 mm, as illustrated in Fig. 1(c).

2.2 Test method

Consolidated undrained (CU) triaxial tests are used to evaluate the impact of initial water content on the shear strength of expansive soil samples under three confining pressures: 50 kPa, 100 kPa, and 200 kPa. The tests are conducted using the GDS stress path triaxial system, as illustrated in Fig. 2(a). Initially, the prepared specimens surrounded by the latex films are placed in the triaxial apparatus, as shown in Fig. 2(b). Subsequently, the distilled water is injected into the triaxial confining chamber to apply the confining pressure. The consolidation phase is considered complete when the excess pore pressure is dissipated and the strain variation is less than 0.125% within a 10-minute interval under the applied confining pressures. Then, the specimens are sheared with an axial strain rate of 0.02%/min, a common setting in experiments (Nan *et al*., 2021), until the axial strain reaches approximately 25%. During the shear loading phase, the drainage valve remains closed.

2.3 Test results

2.3.1 Stress-strain behavior

The deviator stress is plotted as a function of axial strain, as shown in Fig. 3. When the water content is set at 7.65% and 13.78%, the deviator stress of the specimen peaks at certain values and decreases with further axial straining, indicating strain-softening responses. Conversely, at higher water contents of 19.90%, 26.03%, and 31%, the stress-strain curves predominantly exhibit strain-hardening behaviors, where the deviator stress monotonically increases with axial strain. Additionally, an increase in water content is associated with a reduction in peak stress values. In all scenarios, higher confining pressures mitigate strain-softening behavior, and an increase in peak stress values is observed. Low water content typically enhances shear resistance due to the water-generated suction effects. When shear loading disrupts the soil microstructure, this additional shear strength diminishes, leading to strain-softening behavior. However, an increase in water content results in the dissipation of water-generated suctions.

Consequently, the peak shear strength is not as significant as in cases with relatively low water contents, leading to the disappearance of strain-softening behavior. The slope of the initial phase in the stress-strain curve is indicative of the elastic modulus of the expansive soil samples, with the corresponding values for different water contents presented in Fig. 4. It is evident that an increase in the water content tends to reduce the soil elastic modulus.

2.3.2 Shear strength

The shear strength parameters (i.e., cohesion c and friction angle φ) of expansive soil samples under different initial water content conditions can be determined, as shown in Fig. 5, using the Mohr-Coulomb failure envelopes. The variations of cohesion and friction angle can

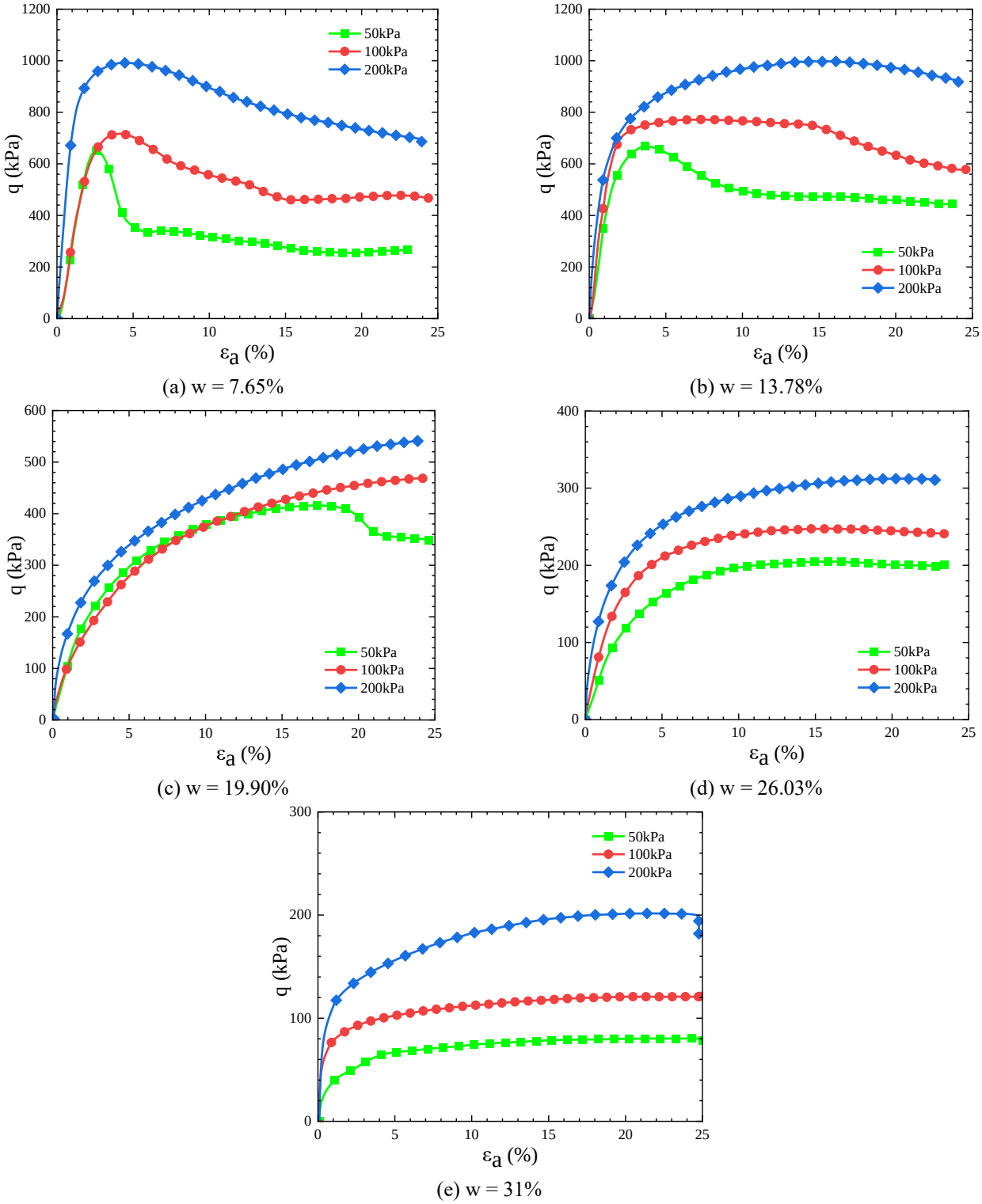

Fig. 3 Stress-strain responses obtained from consolidated undrained triaxial tests on expansive soil samples

be categorized into three zones: Zone A (where w < 13.78%), Zone B (where 13.78% ≤ w <26.03%), and Zone C (where w ≥ 26.03%). With an increase in the initial water content, the cohesion of the expansive soil initially increases from 143.27 kPa to 155.76 kPa (in Zone A) before dropping to 14.91 kPa (in Zones B and C). The presence of water in pores can initially trigger cohesion mobilization in Zone A due to suction effects, as explained in by Chowdhury and Azam (2016). However, as the water content further increases, suction effects gradually dissipate, leading to a rapid cohesion reduction (in Zones B and C), as illustrated by Su *et al*. (2018).

The evolution of friction angle in relation to initial water content follows an inverted S-shape. Specifically, in Zones

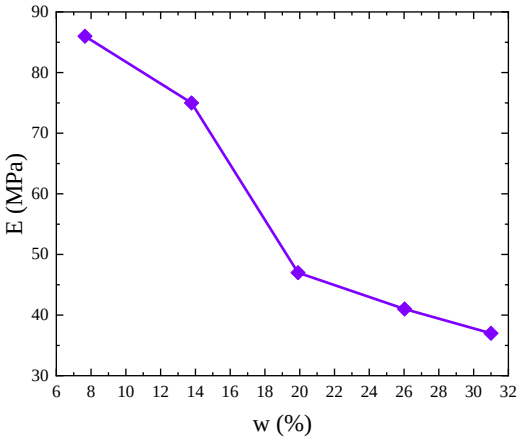

Fig. 4 Elastic modulus in relation to initial water content

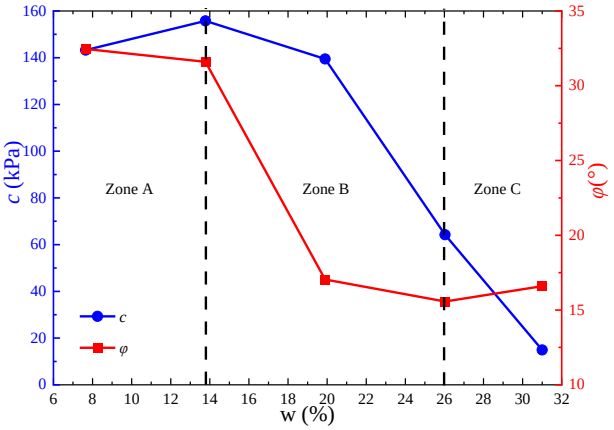

Fig. 5 Strength parameters at different initial water contents

A (relatively low water content) and C (relatively high water content), the friction angle experiences slight changes. However, in zone B, between the two end members, the friction angle decreases sharply from 31.6° to 15.57° with the increase in water content. In Zone A, the limited water in pores has negligible effects on interparticle friction, keeping the friction angle nearly constant. As water content further rises (Zone B), particle contacts are significantly lubricated by water, causing a reduction in the friction angle (Chowdhury and Azam 2016). Finally, when the soil samples approach the saturation state (Zone C), water lubrication ceases to increase, and the friction angle stabilizes again (Su *et al*. 2018). Another worth mentioning aspect is that the cohesion and friction angle of expansive soils decrease by 90% and 49%, respectively, as the initial water content increases from 7.65% to 31%. This indicates that the cohesion of expansive soil is more sensitive to changes in water content compared to the friction angle.

3. Numerical analysis of the bearing behaviour of single pile in expansive soils

To investigate the bearing capacity of a single pile in expansive soils, three-dimensional (3D) numerical simulations are conducted using a commercial finite element modelling platform, ABAQUS (Systèmes, 2014). At the material point level, the Mohr-Coulomb model is used, where the contribution of matric suction to the shear strength parameters of expansive soils is obtained from above CU triaxial tests. Incorporating saturation dependence into advanced geomechanics models can be achieved by explicitly introducing hydraulic variables (e.g., suction and degree of saturation) into the yield function (Alonso *et al*. 1990, Buscarnera and Nova 2009). For example, Mihalache & Buscarnera (2016) developed a constitutive model with a saturation-dependent hardening rule to account for yield surface contraction due to increasing saturation. Besides, considering matrix suction through a more physically acceptable way could be a promising direction of our future work. To achieve this goal, a constitutive model formulated using the thermodynamic analysis should be used as a basis. Then, a grain-size scaling strategy can be applied to both the stress-related and suction-related components of the Helmholtz free energy potential (Buscarnera and Einav 2012), which enables a more physically rigorous manner of capturing the coupling between mechanical and hydraulic properties.

Expansive soils usually swell due to water absorption and shrink if water dissipated, which is analogous to the feature that ordinary materials expand with heating and contract with cooling. In addition, the variation of internal stress and displacement fields of expansive soils caused by the humidity change is similar to those led by temperature change. As a result, the swelling of expansive soils can be modelled by referencing the in-built thermo-mechanical problems. Specifically, the water-induced swelling of expansive soils can be replicated by using the in-built module of thermal-induced material expansive problems through a suitable transition of coefficients. The relation between the humidity linear expansion coefficient α and the temperature linear expansion coefficient β is expressed as:

$$\beta = \frac{\alpha \Delta \mathrm{w}}{\Delta \mathrm{T}} \tag{1}$$

where Δw represents the change in water content, and ΔT represents the temperature change. Notably, Δw and ΔT have the same sign.

Assuming isotropic uniform linear expansion, the humidity linear expansion coefficient α can be computed based on the free swelling ratio of expansive soil

$$\alpha = \frac{\delta_H (1-\nu)}{\Delta \mathrm{w}(1+\nu)} \tag{2}$$

where δ_H denotes the free swelling ratio, and ν represents the Poisson ratio. Due to the same sign of δ_H and Δw, the coefficient α will always remain non-negative. This equation can be further extended to the humidity linear expansion coefficient corresponding to the variation between two specific water contents

$$\alpha_{1,2} = \left| \frac{(\delta_{H2} - \delta_{H1})(1-\nu)}{(\mathrm{w}_2 - \mathrm{w}_1)(1+\nu)} \right| = \left| \frac{\Delta \delta_H (1-\nu)}{\Delta \mathrm{w}(1+\nu)} \right| \tag{3}$$

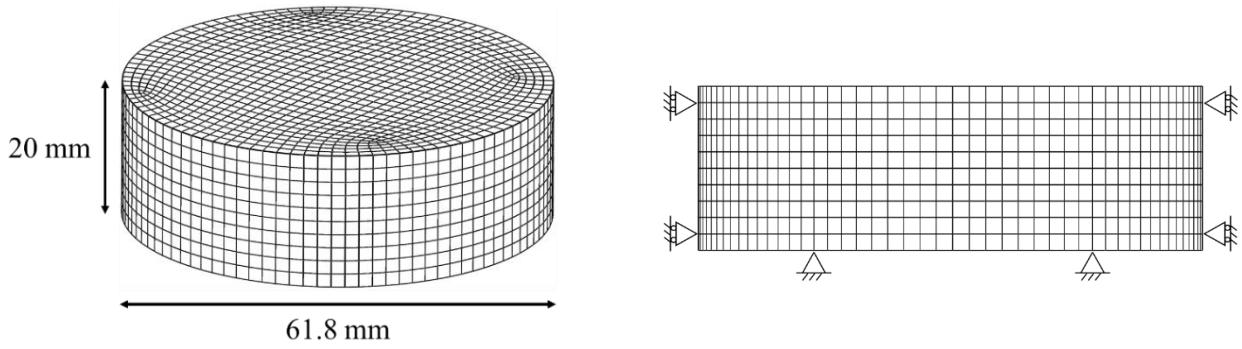

(a) 3D view (b) Front view

Fig. 6 Dimension, spatial discretization, and boundary conditions of the numerical model

Table 1 Experimental data (Zhao *et al*. 2022) and model parameters

Initial water content (%)	Post-swelling water content (%)	Free swelling ratio δ_H (%)	Change in water content Δw (%)	α	β
20	45.536	19.45	25.536	0.3667	0.003667
27	41.11	11.73	14.11	0.4003	0.004003
32	42.88	10.70	10.88	0.4735	0.004735

It is worth mentioning that the swelling and shrinkage of expansive soils due to the water content change can be clearly reflected by the expansion with heating and contraction with cooling in ABAQUS.

3.1 Validation of the simulation method

The free swelling ratio tests of highly swelling soft rocks (SSR) conducted by Zhao *et al*. (2022) are numerically simulated to verify the above simulation strategy. Reconstructed SSR specimens with diameters of 61.8 mm and heights of 20 mm are prepared. The initial water contents are set to 20%, 27%, and 32%, respectively. The free swelling ratio (δ_H) of each specimen is measured after swelling for 24 hours, and the test results from Zhao *et al*. (2022) are presented in Table 1. The Poisson ratio of SSR is not provided. This parameter is assumed to be 0.35, which is a common value for geomaterials.

To explain how to implement the desired simulations in ABAQUS, here the free swelling ratio test of the specimen with an initial water content of 20% is taken as an example. The specific simulation procedure is as follows: (i) the change in water content Δw is 45.536% - 20% = 25.536%, and thus, the humidity linear expansion coefficient α = 0.3667 can be calculated using Eq. (2); (ii) the initial equivalent temperature is set to 20 through the predefined temperature field module of ABAQUS, and is varied to 45.536 in the step of swelling, i.e., the temperature change ΔT is 45.536 – 20 = 25.536; (iii) the temperature linear expansion coefficient β is set to 0.003667 in the material property module, according to Eq. (1). Relevant parameters for the three specimens are summarized in Table 1. In addition, Fig. 6 shows the numerical model of the SSR specimen, which is spatially meshed using 9880 eight-node brick elements. The lateral side is horizontally fixed, and the bottom side is fully constrained according to the requirements of free swell tests.

Fig. 7 presents the vertical displacement contours of these specimens after the swelling. The simulated expansion amounts and the corresponding free swelling ratios are calculated and compared with the experimental results provided by Zhao *et al*. (2022), as summarized in Table 2.

The results reveal that the simulated free swelling ratio is highly close to the measured values, indicating that this simulation method is rational and reliable.

3.2 Model configuration

Fig. 8 shows the model configuration for the bearing capacity analyses of a single pile within expansive soils. The expansive soil body has dimensions of 50 m × 50 m × 50 m, and the single pile within it measures 27 m in length and 2 m in diameter. The numerical simulation procedure consists of three steps. In the first step, the initial geostatic stress is generated by applying gravity, and a predefined temperature field with a value of 18 is set to the entire soil body. In the second step, the equivalent temperature of soil within the atmospheric influence depth is modified to specific values, allowing for soil shrinkage or swelling. In the third step, a downward displacement of 0.5 m which increases linearly from 0 is applied to the pile top. The numerical model is spatially discretized using 57200 eight-node brick elements, with a relatively finer mesh used around the pile-soil interface for accuracy. This mesh configuration can balance accuracy and numerical costs. Further refinement of mesh has negligible effects on the simulated load-displacement response, but remarkably increases the computational time.

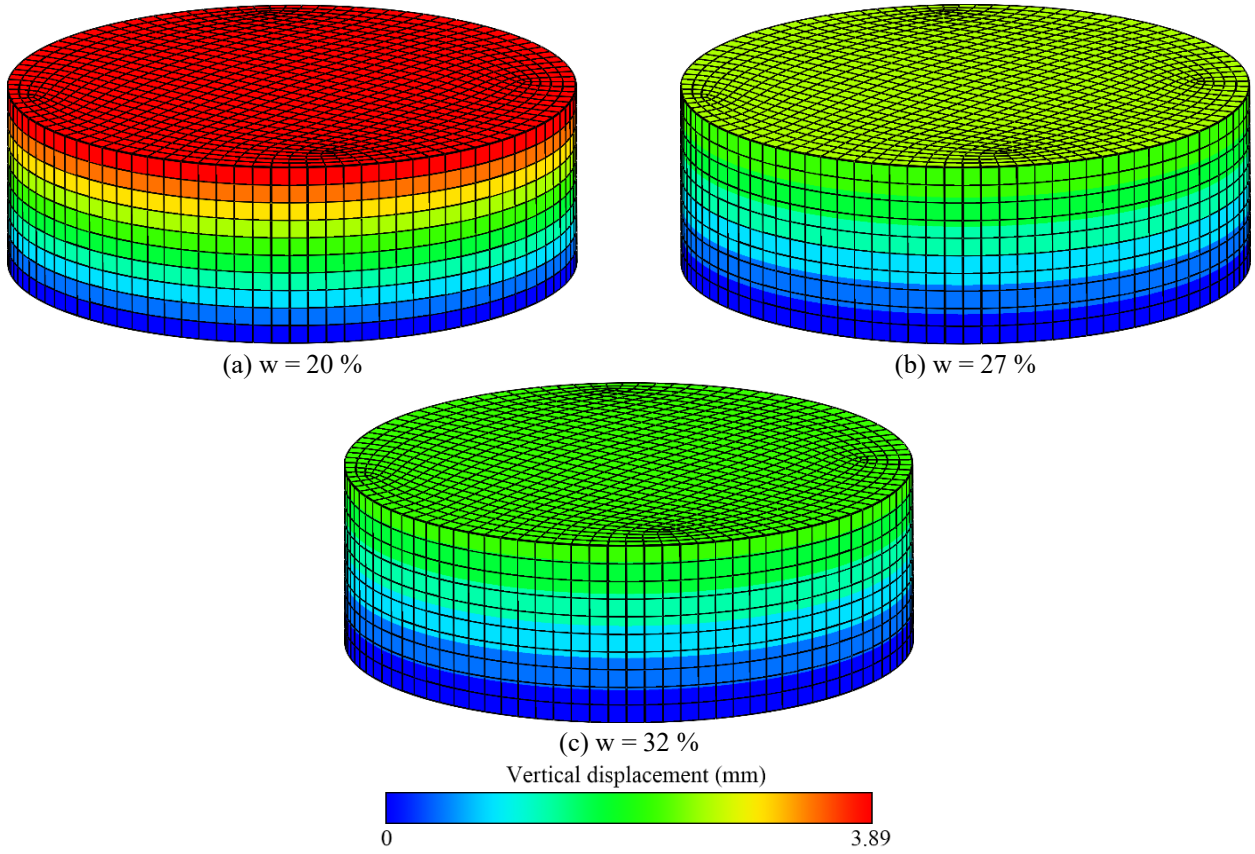

Fig. 7 Displacement contours of SSR specimens with different initial water contents after the swelling

Table 2 Comparison between the simulated and experimental results

Initial water content (%)	Simulated swelling amount (mm)	Simulated swelling ratio (%)	Measured free swelling ratio (%)
20	3.88968	19.4484	19.45
27	2.34619	11.7310	11.73
32	2.13993	10.6997	10.70

Table 3 Model parameters for the expansive soil and pile

Unit weight (kN/m^3)		Modulus of Elasticity (MPa)		Poisson ratio (μ)	
Soil	Pile	Soil	Pile	Soil	Pile
20.7	25	See Table 4	20000	0.35	0.31

Table 4 Specific parameters for the expansive soil at different water contents

Water content w (%)	Elastic modulus E (MPa)	Cohesion c (kPa)	Friction angle φ (°)
7.65	86	143.27	32.46
13.78	75	155.76	31.60
18.00	65	139.63	20.41
19.90	47	139.44	17.04
26.03	41	64.23	15.57
31.00	37	14.91	16.60

It has been reported that the pile-soil interaction may significantly affect the mechanical performance of the pile foundation (Aksoy *et al*. 2016). A contact law is applied at the pile-soil interface, featuring hard contact in the normal direction and a penalty contact with a coefficient of tan (0.75 φ) set tangentially. Besides, nodes at the horizontal boundaries are fixed from moving laterally, and nodes at the bottom boundary are fully fixed. The soils and pile are assumed to follow the elastoplastic Mohr-Coulomb model and pure elastic model, respectively. Tables 3 and 4 present the relevant model parameters for expansive soils and the pile. Notably, the model parameters for the pile are taken based on the empirical values of reinforced concrete. As for the expansive soil, the unit weight and Poisson's ratio are taken from the laboratory tests, and the elastic modulus, friction angles, and cohesions are obtained from the triaxial tests presented previously.

Previous studies (Azam and Ito 2012, Adem and Vanapalli 2016, Wu and Vanapalli 2022) have demonstrated the existence of an atmospheric influence depth, below which the water content and temperature of the expansive soils stabilize at certain values. As a result, the expansive soils below this influence depth usually can be considered to have reached a stable state and the relevant material parameters are minimally affected by far-field drying or wetting processes. Field investigation in the sampled region indicates that the atmospheric influence depth ranges from 5.1 to 5.3 m, and the water content below this depth

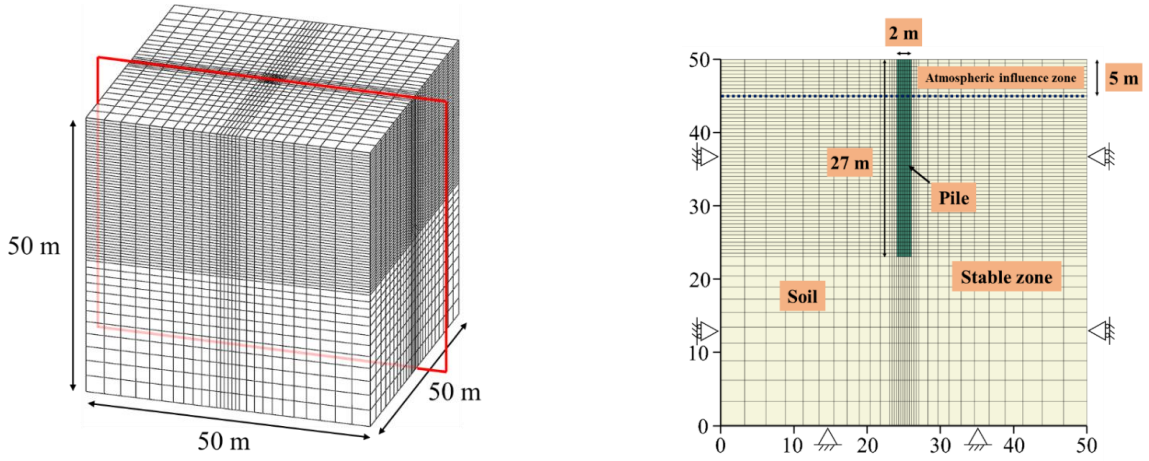

(a) Expansive soil body (b) A cross-section showing the single pile

Fig. 8 Geometry, spatial discretization, and boundary conditions for the numerical model

Table 5 Calculation of the linear expansion coefficients corresponding to different variations of water contents in the atmospheric influence zone

w_1 (%)	w_2 (%)	δ_{H1} (%)	δ_{H2} (%)	$\Delta\delta_H$ (%)	Δw (%)	α	β
18	7.65	14.067	31.455	17.388	- 10.35	0.8089	0.008089
18	13.78	14.067	24.910	10.843	- 4.22	1.2372	0.012372
18	18	14.067	14.067	0	0	0	0
18	19.9	14.067	9.654	- 4.413	1.90	1.1183	0.011183
18	26.03	14.067	1.859	- 12.208	8.03	0.7320	0.007320
18	31	14.067	- 0.195	- 14.262	13.00	0.5282	0.005282

maintains approximately 18%. In the numerical model, the atmospheric influence depth is thus set at 5 m, with the water content beneath this depth fixed at 18%. For the regions above the atmospheric influence depth, the water content for all soils changes simultaneously from the natural value (18%) to a specific value, see Table 4, a simplified strategy conforming to the engineering scenario. Besides, a reference case is set where the water content of the entire expansive soil body always maintains at 18%. Table 5 summarizes the required linear expansion coefficients in the simulation based on Eqs. (1)-(3), where the free swelling ratios at different initial water contents are extracted from Su *et al*. (2018).

3.3 Deformation mode

In the simulation, a vertical displacement-controlled loading is applied to the pile top until the ultimate bearing capacity of the soil foundation is reached. The equivalent plastic strain maps at the ultimate state are demonstrated in Fig. 9. It can be seen from the figure that a concentrated spherical-shaped plastic deformation zone occurs around the pile bottom due to the vertical loading, while the water content has negligible effects on this plastic region, which is attributed to the same water content of 18% below the atmospheric influence depth. However, the soils within the atmospheric influence depth exhibit plastic strain due to the shrinkage or swelling caused by the changing water content, and the equivalent plastic strain will increase when the variation of water content becomes more significant.

To further explore the deformation mode of the foundation at the ultimate state of soils, Fig. 10 presents the displacement maps and vector diagram. In all cases, soils around the pile bottom exhibit settlement under loading, with a maximum value of approximately 0.5 m. When the water content within the atmospheric influence depth is at 7.65% or 13.78%, noticeable soil shrinkages can be observed, which leads to the position separation of the pile and soils. The maximum soil shrinkage displacements occur near the ground surface, measuring 2.363 m and 1.454 m at the water content of 7.65% and 13.78%, respectively. When the water content is set at 18%, corresponding to the same value as the soils beneath the influence depth, the soils within the atmospheric influence depth neither swell nor shrink. With the water content set to 19.90%, 26.03%, or 31%, the soils within atmospheric influence depth swell, leading to visible ground uplift. The maximum uplift of soils increases with the water content, measuring 0.510 m, 1.275 m, and 1.516 m at the water content of 19.90%, 26.03%, and 31%, respectively.

3.4 Ultimate bearing capacity

Fig. 11(a) illustrates the load-displacement responses of the single pile under different water content conditions in the atmospheric influence zone. The simulated curves

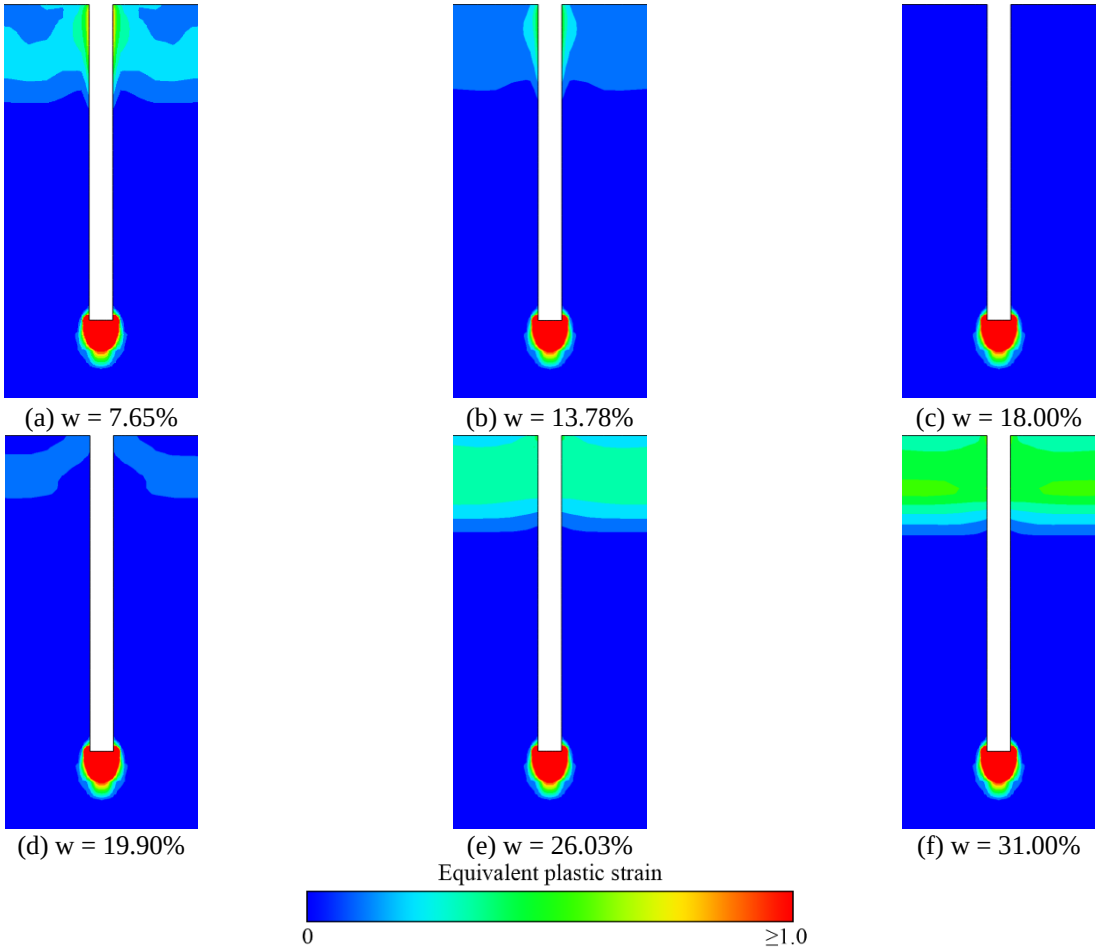

Fig. 9 Equivalent plastic strain maps of expansive soil foundation with different water contents in the atmospheric influence zone

exhibit a similar trend, i.e., the load magnitude increases with the increasing displacement of the pile. When the load reaches threshold values, the soils can exhibit infinite displacement. These threshold values are considered as the ultimate bearing capacity of the pile. The variation of ultimate bearing capacity of the pile with respect to different water contents within the atmospheric influence depth is shown in Fig. 11(b). It can be observed that the ultimate bearing capacity of the pile with water contents of 7.65% and 13.78% are extremely close. This phenomenon can be attributed to the fact that, when the used water content is below the natural water content (18%), the lateral frictional resistance along the upper part of the pile is minimal due to the soil-shrinkage-induced separation of the pile and soil. Consequently, the load is mainly taken by the pile bottom resistance and the lateral friction below the atmospheric influence depth. However, with a further increase in water content, the ultimate bearing capacity initially increases and then decreases. In fact, despite the swelling of soils within the atmospheric influence depth contributing to increased lateral frictional resistance and ultimate bearing capacity, the shear strength parameters of expansive soil decrease with water content. As a result, the ultimate bearing capacity does not exhibit a monotonic increase with the water content, yet remains higher than that for cases with water contents lower than 18% (the natural value).

4. Numerical analysis of pile uplift potential under soil swelling

4.1 Estimation of swelling shear stress

The swelling of an expansive soil body due to the absorption of water can generate upward shear force (i.e., swelling force) to the pile sides, as shown in Fig. 12. This phenomenon can potentially result in pile uplifts and damage surface structures. Therefore, it is crucial to determine the force magnitude required to be applied to the pile top, for the purpose of eliminating possible pile uplifts. To achieve this goal, the determination of swelling force is needed.

In practical engineering, the computation of the swelling force mainly relies on field tests. Specifically, the expansive soil, containing a single pile, is allowed to swell under different water contents, while the pile top is constrained to measure the forces of interest. However, field tests are usually time-consuming, making the numerical analysis strategy a viable alternative for estimate the expansion force

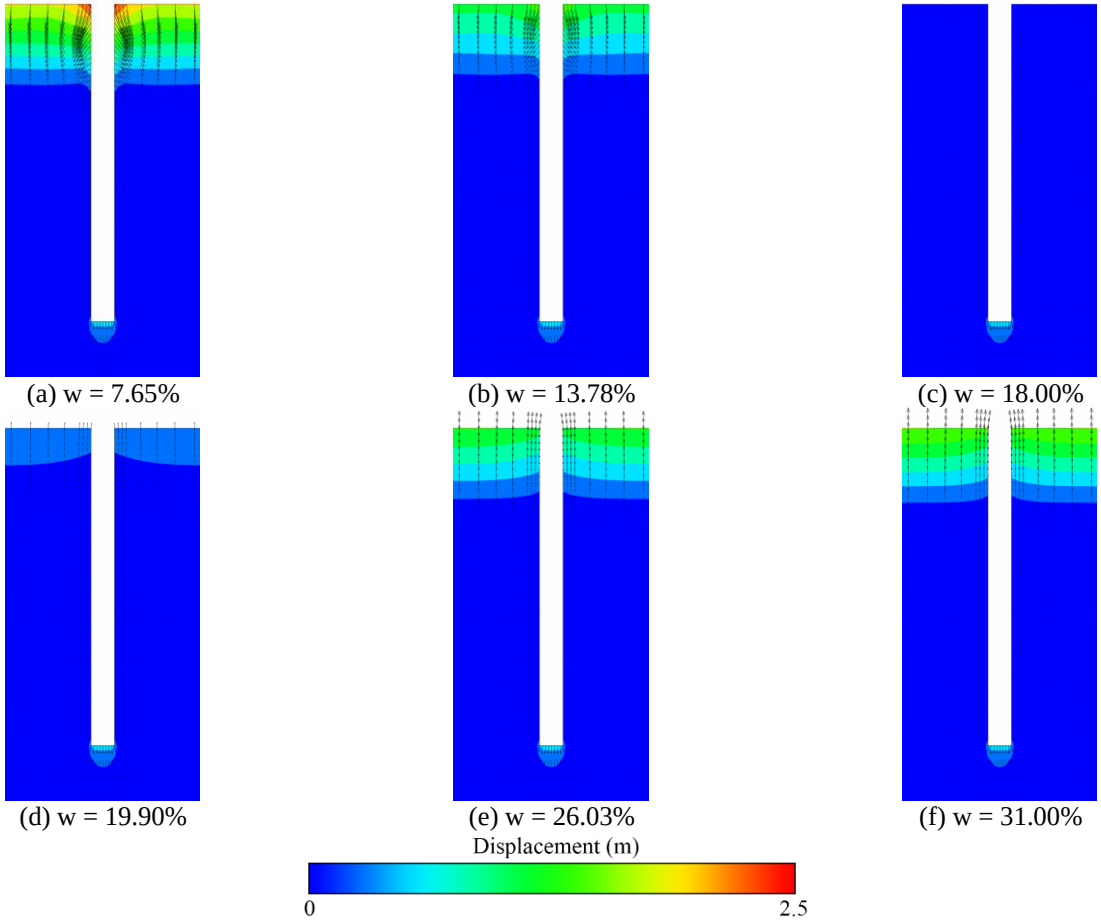

Fig. 10 Displacement maps and vector diagram of expansive soil foundation with different water contents in the atmospheric influence zone

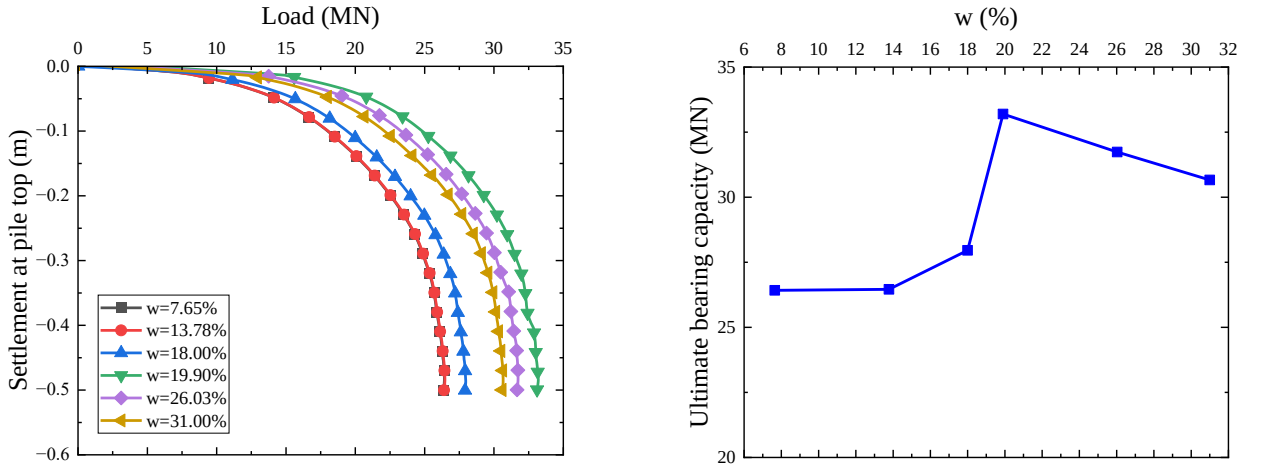

(a) Load-displacement curves

(b) Variation of ultimate bearing capacity with respect to water content in the atmospheric influence zone

Fig. 11 Bearing capacity of the pile in the expansive soils

experienced by the pile. This, in turn, offers guidance for engineering designs and optimizations.

By modifying the numerical model presented in Section 3 according to field tests in terms of the boundary conditions, a numerical analysis of swelling shear stress can be conducted, and the reaction force at the pile top under soil swelling effects can be therefore measured. Herein, the numerical simulation includes two steps: (i) the initial geostatic stress is generated with applied gravity, and an initial predefined temperature field is also established for

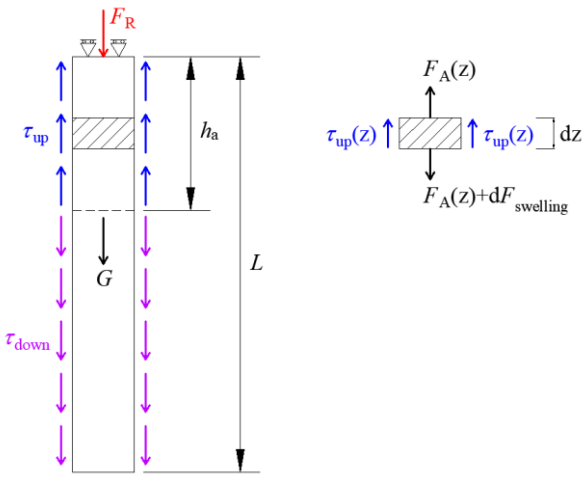

Fig. 12 Schematic of force balance of the pile in the expansive soil body

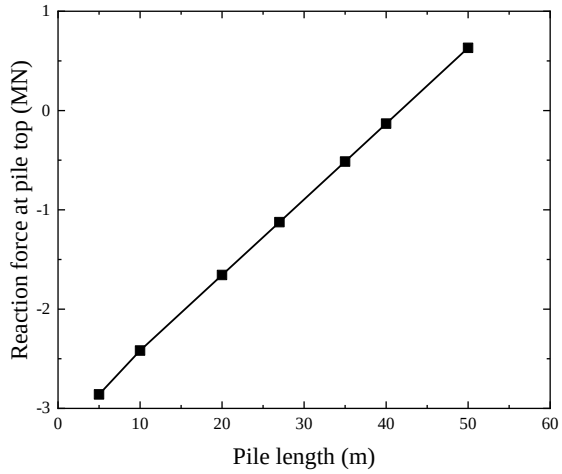

Fig. 13 Reaction force of pile top with respect to pile length

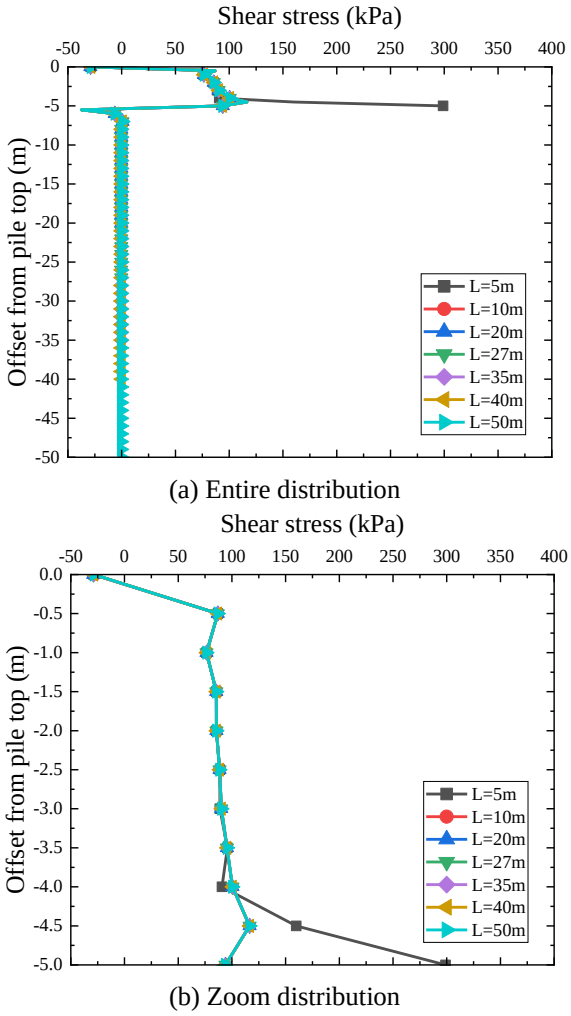

Fig. 14 Distribution of shear stress with different pile lengths

the entire soil body, and (ii) the equivalent temperature of soil within the atmospheric influence depth is raised to another value, which represents the increase in water content. In the step (ii), the pile top remains constrained.

The force balance schematic of the pile is shown in Fig. 12, indicating that the swelling force increment on a unit extracted from the region within the atmospheric influence depth can be expressed as follows

$$dF_{swelling}(z) = \pi D \tau_{up}(z) dz \tag{4}$$

and the total swelling force can be finally derived:

$$F_{swelling} = \int_0^{h_a} \pi D \tau_{up}(z) dz = \pi D \int_0^{h_a} \tau_{up}(z) dz \tag{5}$$

where $F_{swelling}$ (z) and τ_{up} (z) denote the swelling force and the shear stress at a depth of z, respectively. F_A (z) represents the axial force at a depth of z, h_a represents the depth of atmospheric influence (h_a = 5 m in this study), and D represents the pile diameter. In the following sections, the effects of pile length, diameter, and soil water content on the swelling shear stress distribution and total swelling force are investigated.

4.2 Effects of pile length

When the pile length exceeds the atmospheric influence depth, both the pile self-weight and the pullout resistance provided by the soil body below the atmospheric influence depth increase with the pile length. This may potentially prevent the expansive-effects-induced pile uplift. As a result, there exists an optimal pile length beyond which the reaction force at the pile top reaches zero. In other words, if this optimal pile length is used, the swelling force counteracts the self-weight of pile and the pullout resistance provided by the soils below the atmospheric influence depth. To numerically determine this optimal pile length, various pile lengths (L) are considered, namely 5, 10, 20, 27, 35, 40, and 50 m, respectively. The pile diameter (D) is fixed at 2.0 m, and the water content of the expansive soil body within the atmospheric influence depth is set at 20% (slightly higher than the natural water content 18%), ensuring the generation of the swelling force.

The simulated reaction force at pile top is plotted against the pile length, as shown in Fig. 13. It is observed that when the pile has a length of 5m, the reaction force at pile top reaches -2859.3 kN (negative sign indicates compression).

Table 6 Integration of shear stress and the corresponding swelling force with different pile lengths

Pile length (m)	Integration from 0 to -5 m (kN/m)	Total swelling force (kN)
5	496.730	3121.047
10	428.721	2693.733
20	428.905	2694.890
27	428.977	2695.342
35	429.162	2696.504
40	429.190	2696.680
50	429.215	2696.837

As the pile length increase, the reaction force at pile top decreases, and eventually becomes positive, indicating tension. This indicates that the swelling force is insufficient to generate pile uplift movement. According to the simulations, the optimal pile length resulting in 0 reaction force at pile top is predicted to be approximately 41.7 m.

The shear stress distribution along the pile is shown in Fig. 14(a). Within the atmospheric influence depth, the shear stress is positive, indicating that this part of pile is subjected to an upward friction provided from soils due the soil swelling effects. In contrast, the shear stress remains negative below the atmospheric influence depth, and gradually vanishes with increasing depth. The expansive soil body below the atmospheric influence depth generates downward frictional resistance along the pile, but the magnitude of this friction is relatively small. Fig. 14(b) presents the zoom shear stress distribution. While the case with a pile length of 5 m exhibits relatively high shear stress near the atmospheric influence depth, other cases demonstrated almost identical distributions of shear stress. The integration of shear stress from 0 m to -5 m and the corresponding total swelling force are summarized in Table 6. It is shown that both the integration of shear stress over the atmospheric influence depth and the swelling force in any given soil unit within atmospheric influence depth is nearly unaffected by the pile length.

4.3 Effects of pile diameter

In this section, in the context of soil swelling, the effects of pile diameter on the pile uplift are studied. The pile length is selected as 27 m, the water content of the expansive soil body within the atmospheric influence depth is set at 20%, and the pile diameter is varied as 0.5, 1.0, 1.5, 2.0, 2.5, 3.0, 4.0, and 5.0 m, respectively. Fig. 15 presents the variation of reaction force at the pile top with respect to pile diameter at the end of the simulation. The reaction force at the pile top initially increases from -636.8 kN to -1202.7 kN, as the pile diameter increases. In this stage, the growth in pile diameter corresponds to the increase in pile uplift potential outweighing the increase in the pile self-weight. However, with a further increase at pile diameter, the contribution of pile self-weight is more remarkable than the pile uplift potential, leading to a reduction of reaction

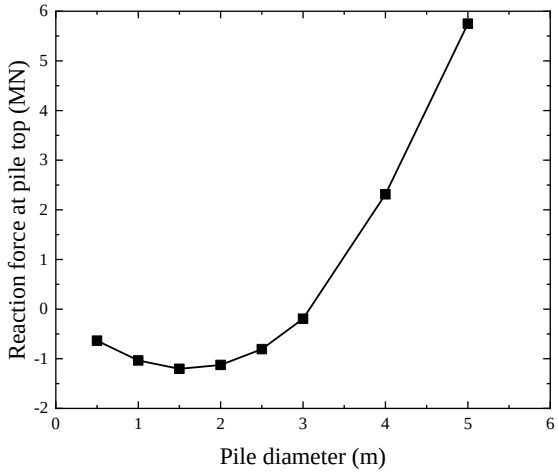

Fig. 15 Reaction force of pile top with respect to pile diameter

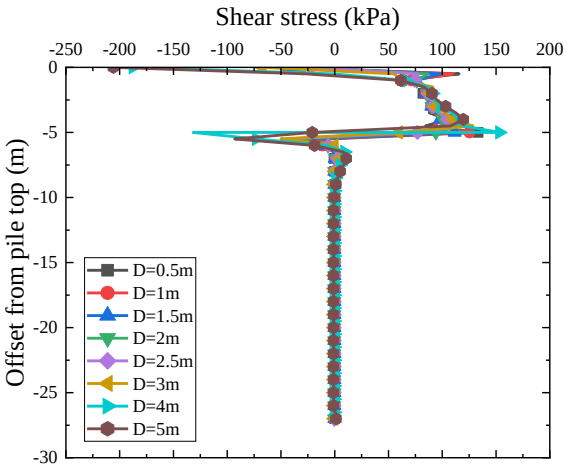

(a) Entire distribution

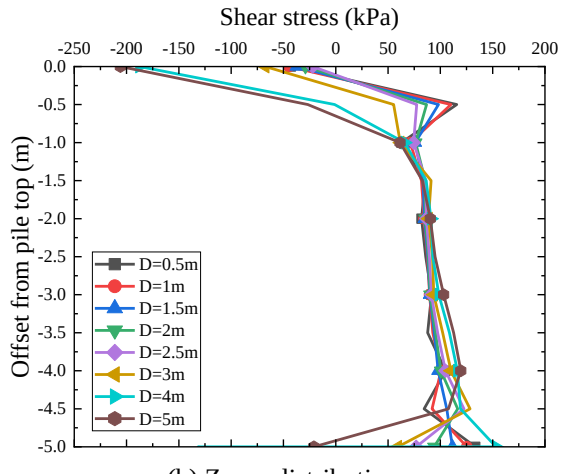

(b) Zoom distribution

Fig. 16 Distribution of shear stress with different pile diameters

force at pile top. The reaction force reaches approximately 0 kN, when the pile has a diameter of 3 m, indicating that the swelling effects is insufficient to generate pile uplift potential. By observing Fig. 15, the most dangerous pile diameter (i.e., the highest compressive reaction force) and

Table 7 Integration of shear stress and the corresponding swelling force with different pile diameters

Pile diameter (m)	Integration from 0 to -5 m (kN/m)	Total swelling force (kN)
0.5	423.038	664.507
1.0	425.394	1336.415
1.5	427.829	2016.097
2.0	428.977	2695.342
2.5	428.859	3368.251
3.0	409.795	3862.227
4.0	380.384	4780.046
5.0	316.382	4969.717

the optimal pile diameter (i.e., reaction force at zero) is predicted to be approximately 1.58 m and 3.0 m, respectively.

The shear stress distributions along the pile are presented in Fig. 16(a). Within the atmospheric influence depth, the shear stress almost remains positive, reflecting the upward swelling stress on this part of pile. In contrast, the shear stress exhibits a negative sign within the soil region below the atmospheric influence depth because the expansive soils in the stable zone provides downward friction to the pile. The shear stress gradually reduces to 0 with the increase in depth. Fig. 16(b) presents the zoom shear stress distribution within the atmospheric influence depth. When the pile diameter ranges from 0.5 m to 3.0 m, the distributions of shear stress exhibit similar behavior. In the cases with pile diameters of 4.0 m and 5.0 m, the shear stress near the pile top drops. The integration of shear stress from 0 m to -5 m and the corresponding swelling force are summarized in Table 7. Although integration of the shear stress from 0 m to -5 m does not show a noticeable change with pile diameter, the computed total swelling force heavily depends on the pile diameter, and increase from 664.5 kN to 4969.7 kN when the pile diameter increases from 0.5 m to 5.0 m.

4.4 Effects of water content

Water content is another crucial factor that needs to be explored. Here, the variation of the shear stress with respect to water content is numerically studied. The numerical simulations consider six different water contents for the atmospheric influence depth, i.e., 20%, 22%, 24%, 26%, 28%, and 31%. The corresponding shear strength parameters and swelling ratios are obtained through interpolation based on Tables 4 and 5. The pile length and diameter are selected as 27 m and 2 m. Fig. 17 shows that the compressive force at pile top decreases as the water content increases. When the water content increases to approximately 24.5%, the reaction force at pile top become negligible, indicating that there is no need to consider the pile uplift potential provided from soil swelling effects when the water content within the atmospheric influence depth exceeds this critical value. In fact, as the water content increases, soil swelling effects become more

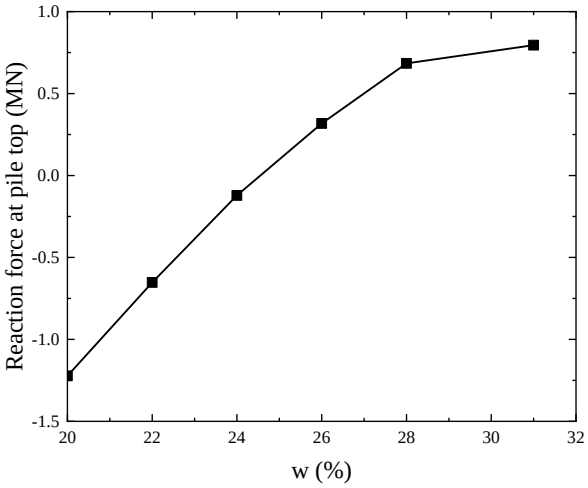

Fig. 17 Reaction force of pile top with respect to water content in the atmospheric influence zone

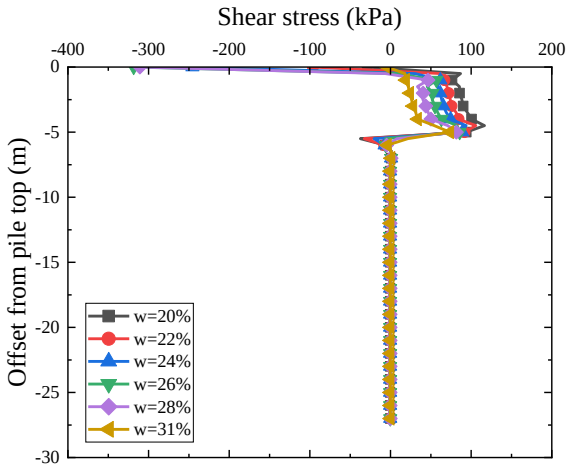

(a) Entire distribution

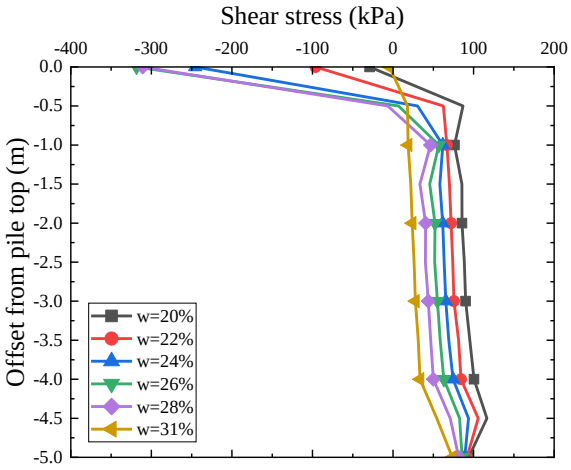

(b) Zoom distribution

Fig. 18 Distribution of shear stress with different water contents in the atmospheric influence zone

pronounced, leading to an increase in pile-soil relative displacement. In the meantime, however, with the increase in water content, the shear strength parameters of the soil show decreasing trends. Eventually, the latter effects

Table 8 The integration of shear stress and the corresponding swelling force with different water contents in the atmospheric influence zone

Water content (%)	Integration from 0 to -5 m (kN/m)	Total swelling force (kN)
20	428.977	2695.342
22	345.371	2170.030
24	250.149	1571.733
26	178.128	1119.211
28	125.689	789.727
31	145.116	911.791

overwhelm the former effects, and the reaction force at the pile top keeps dropping along the water content.

5. Conclusions

In this paper, the bearing behavior and uplift potential of a single pile in expansive soils are numerically studied. To this end, the effects of water contents on the mechanical behavior and shear strength are examined through a series of consolidated undrained (CU) triaxial tests. Subsequently, the obtained dataset is used to drive the establishment of a three-dimensional (3D) finite element (FE) model of a single pile in expansive soils, where the soil swelling/shrinkage behavior is properly simulated via the user-defined thermal-mechanical coupling module in ABAQUS. On this basis, soil deformation modes and the bearing capacity of the pile are assessed. The FE numerical model is further modified to investigate the effects of pile length, diameter, and water content on pile uplift potential during soil swelling. The main conclusions drawn from this work are as follows:

• Triaxial test results reveal that with the increase in water content the cohesion of expansive soils initially increases slightly and then decreases sharply. Meanwhile, the friction angle undergoes a slight initial change, followed by a significant decrease, and ultimately stabilizes.

• Numerical analyses are conducted based on the Mohr-coulomb constitutive model, where the variation of its parameters along water contents is considered using the experimental data. The delicate link of the water-induced swelling and shrinking to those caused by temperature change allows for the modeling of soil swelling-shrinkage behavior regarding water content to be achieved by the thermo-mechanical module of ABAQUS through proper definitions of material parameters. Correspondingly, the temperature field can be made analogous to the water content. The proposed implementation strategy is validated by simulating the free swelling ratio tests of highly swelling soft rocks.

• Numerical simulations show that greater increases or decreases in water content within the atmospheric influence depth cause more significant swelling or shrinkage deformation. When the water content within this depth drops below the natural value, the pile ultimate bearing capacity experiences a slight decrease due to pile-soil separation caused by soil shrinkage. However, it increases sharply when the water content surpasses the natural water content, thanks to the upward friction applied by the expansive soils to the pile due to soil swelling effects. Subsequently, the ultimate bearing capacity declines as the water content continues to rise, as the effects of soil strength reduction overwhelm the influences of upward soil-to-pile friction.

• An increase in pile length leads to higher pile self-weight and downward settling effects, transforming the reaction force at the pile top from compression to tension, indicating the decrease of pile uplift potential. An increase in pile diameter raises both the upward soil-to-pile friction and pile self-weight. Consequently, due to the competing mechanism of these two effects, as the pile diameter grows, the pile uplift potential initially increases, followed by a decrease phase. Increasing water content within the atmospheric influence depth enhances the pile-soil relative movement while decreasing shear strength parameters. Eventually, the effects of soil strength reduction overwhelm swelling effects, and the evolution of the reaction force at the pile top reflects a diminished pile uplift potential with increasing water content.

Acknowledgments

The financial supports by Guangxi Science and Technology Major Program (Grant No. 2022AA15001) are gratefully acknowledged.

References

Abden, A., Al-Shamrani, M., Dafalla, M. and Siddiqui, N. (2024), "Assessment of the performance of spread footings and mat foundations on expansive soils", *Results Eng.*, **23**, 102782. https://doi.org/10.1016/j.rineng.2024.102782.

Adem, H. and Vanapalli, S. (2016), "Soil-environment interactions modelling for expansive soils", *Environ. Geotech.*, **3**(3), 178-187. https://doi.org/10.1680/envgeo.13.00089.

Aksoy, H., Gör, M. and İnal, E. (2016), "A new design chart for estimating friction angle between soil and pile materials", *Geomech. Eng.*, **10**(3), 315-324. https://doi.org/10.12989/GAE.2016.10.3.315.

Alnmr, A., Ray, R.P. and Alsirawan, R. (2023), "A state-of-the-art review and numerical study of reinforced expansive soil with granular anchor piles and helical piles", *Sustainability*, **15**(3), 2802. https://doi.org/10.3390/su15032802.

Alnmr, A., Ray, R. and Alzawi, M.O. (2024), "Comparative analysis of foundation systems in expansive soil: a three-dimensional model approach to moisture diffusion and volume changes", *Geotech. Geol. Eng.*, **42**(8), 7935-7961. https://doi.org/10.1007/s10706-024-02959-2.

Alonso, E.E., Gens, A. and Josa, A. (1990), "A constitutive model for partially saturated soils", *Géotechnique*, **40**(3), 405-430. https://doi.org/10.1680/geot.1990.40.3.405.

Al-Yaqoub, T. H., Parol, J. and Znidarcic, D. (2017), "Experimental investigation of volume change behavior of swelling soil", *Appl. Clay Sci.*, **137**, 22-29.

https://doi.org/10.1016/j.clay.2016.11.018.
Awadalseed, W., Zhang, X., Ji, Y., Wang, X., Bai, Y. and Zhao, H. (2024), "Experimental and numerical simulation study of water infiltration impact on soil-pile interaction in expansive soil", *Geofluids*, **2024**(1), 6642676. https://doi.org/10.1155/2024/6642676.
Azam, S. and Ito, M. (2012), "Coupled soil-atmosphere modeling for expansive regina clay", *J. Environ. Inform.*, **19**(1), 20-29. https://doi.org/10.3808/jei.201200205.
Aziz, M., Saleem, M. and Irfan, M. (2015), "Engineering behavior of expansive soils treated with rice husk ash", *Geomech. Eng.*, **8**(2), 173-186. https://doi.org/10.12989/gae.2015.8.2.173.
Bai, F. and Liu, S. (2012), "Measurement of the shear strength of an expansive soil by combining a filter paper method and direct shear tests", *Geotech. Test. J.*, **35**(3), 451-459. https://doi.org/10.1520/GTJ103342.
Bhaduri, A. and Choudhury, D. (2020), "Serviceability-based finite-element approach on analyzing combined pile–raft foundation". *Int. J. Geomech*., **20**(2), 04019178. https://doi.org/10.1061/(ASCE)GM.1943-5622.0001580.
Burke, T.S.d.S., Jacobsz, S.W., Elshafie, M.Z.E.B. and Osman, A.S. (2022), "Measurement of pile uplift forces due to soil heave in expansive clays", *Can. Geotech. J.*, **59**(12), 2119-2134. https://doi.org/10.1139/cgj-2021-0079.
Buscarnera, G. and Einav, I. (2012), "The yielding of brittle unsaturated granular soils", *Géotechnique*, **62**(2), 147-160. https://doi.org/10.1680/geot.10.P.118.
Buscarnera, G. and Nova, R. (2009), "An elastoplastic strain hardening model for soil allowing for hydraulic bonding–debonding effects", *Int. J. Numer. Anal. Method. Geomech.*, **33**(8), 1055-1086. https://doi.org/10.1002/nag.756.
Chowdhury, R.H. and Azam, S. (2016), "Unsaturated shear strength properties of a compacted expansive soil from Regina, Canada", *Innov. Infrastruct. Solut.*, **1**, 47. https://doi.org/10.1007/s41062-016-0047-2.
Fan, Z.H., Wang, Y.H., Xiao, H.B. and Zhang, C.S. (2007), "Analytical method of load-transfer of single pile under expansive soil swelling", *J. Cent. South Univ. Technol.*, **14**(4), 575-579. https://doi.org/10.1007/s11771-007-0110-4.
Fattah, M.Y., Al-Mosawi, M.J. and Al-Zayadi, A.A.O. (2013), "Time dependent behavior of piled raft foundation in clayey soil", *Geomech. Eng.*, **5**(1), 17-36. https://doi.org/10.12989/GAE.2013.5.1.017.
Fredlund, D., Morgenstern, N. and Widger, R. (1978), "The shear strength of unsaturated soils", *Can. Geotech. J.*, **15**(3), 313-321. https://doi.org/10.1139/t78-029.
GB 50112 (2013), "Technical code for buildings in expansive soil regions", Chinese Standard.
Hou, K.W., Jiang, J., Wang, S.W. and Ou, X.D. (2021), "Physical model test and theoretical study on the bearing behavior of pile in expansive soil subjected to water infiltration", *Int. J. Geomech.*, **21**(6), 06021014. https://doi.org/10.1061/(ASCE)GM.1943-5622.0002006.
Iizuka, A., Tachibana, S., Takeyama, T., Sugiyama, Y., Nomura, S. and Ohta, H. (2019), "Extension of unsaturated soil mechanics and its applications", *Geotech. Res.*, **6**(3), 156-176. http://doi.org/10.1680/jgere.18.00004.
Jain, A.K. and Jha, A.K. (2020), "Geotechnical behaviour and micro-analyses of expansive soil amended with marble dust", *Soils Found.*, **60**(4), 737-751. https://doi.org/10.1016/j.sandf.2020.02.013.
Khanmohammadi, M. and Fakharian, K. (2018), "Evaluation of performance of piled-raft foundations on soft clay: A case study", *Geomech. Eng.*, **14**(1), 43-50. https://doi.org/10.12989/GAE.2018.14.1.043.
Lavanya, C. and Kumar, N.D. (2021), "Effect of lime-stabilised copper slag cushion on swelling behaviour of highly plastic clay", *Geotech. Res.*, **9**(1), 15-22. http://doi.org/10.1680/jgere.21.00006a.
Liu, Y. and Vanapalli, S.K. (2017), "Influence of lateral swelling pressure on the geotechnical infrastructure in expansive soils", *J. Geotech. Geoenviron. Eng.*, **143**(6), 04017006. https://doi.org/10.1061/(ASCE)GT.1943-5606.0001651.
Liu, Y. and Vanapalli, S.K. (2019), "Load displacement analysis of a single pile in an unsaturated expansive soil", *Comput. Geotech.*, **106**, 83-98. https://doi.org/10.1016/j.compgeo.2018.10.007.
Liu, Y. and Vanapalli, S.K. (2021), "Mechanical behavior of a floating model pile in unsaturated expansive soil associated with water infiltration: Laboratory investigations and numerical simulations", *Soils Found.*, **61**(4), 929-943. https://doi.org/10.1016/j.sandf.2021.06.004.
Liu, Y., Vanapalli, S.K. and Jiang, S. (2022), "Mechanical behavior of piles in typical unsaturated expansive and collapsible soils upon water infiltration", *Front. Built Environ.*, **8**, 864421. https://doi.org/10.3389/fbuil.2022.864421.
Miao, L., Liu, S. and Lai, Y. (2002), "Research of soil–water characteristics and shear strength features of Nanyang expansive soil", *Eng. Geol.*, **65**(4), 261-267. https://doi.org/10.1016/S0013-7952(01)00136-3.
Mihalache, C. and Buscarnera, G. (2016), "Controllability criteria for soils saturated by a compressible fluid", *J. Eng. Mech.*, **142**(10): 04016076. https://doi.org/10.1061/(ASCE)EM.1943-7889.0001137.
Mohanty, S., Pradhan, P. and Mohanty, C. (2017), "Stabilization of expansive soil using industrial wastes", *Geomech. Eng.*, **12**(1), 111-125. https://doi.org/10.12989/GAE.2017.12.1.111.
Nan, J., Peng, J., Zhu, F., Ma, P., Liu, R., Leng, Y. and Meng, Z. (2021), "Shear behavior and microstructural variation in loess from the Yan'an area, China", *Eng. Geol.*, **280**, 105964. https://doi.org/10.1016/j.enggeo.2020.105964.
Nelson, J.D., Thompson, E.G., Schaut, R.W., Chao, K.C., Overton, D.D. and Dunham-Friel, J.S. (2012), "Design procedure and considerations for piers in expansive soils", *J. Geotech. Geoenviron. Eng.*, **138**(8), 945-956. https://doi.org/10.1061/(asce)gt.1943-5606.0000647.
Su, Z., Qi, D., Guo, X., Xi, X. and Zhang, L. (2018), "Characterization of the undrained shear strength of expansive soils of High water content", *MATEC web of conferences*, **206**, 01002. https://doi.org/10.1051/matecconf/201820601002.
Systèmes, D. (2014), "Abaqus user subroutines reference guide, version 6.14", *Dassault Systemes Simulia Corp., Providence, RI*, USA.
Wei, M., Liao, F., Zhou, K., Yan, S., Liu, J. and Wang, P. (2022), "Influence of moisture content on main mechanical properties of expansive soil and deformation of non-equal-length double-row piles: A case study", *Geomech. Eng.*, **30**(2), 139-151. https://doi.org/10.12989/gae.2022.30.2.139.
Wu, X. and Vanapalli, S.K. (2022), "Three-dimensional modeling of the mechanical behavior of a single pile in unsaturated expansive soils during infiltration", *Comput. Geotech.*, **145**, 104696. https://doi.org/10.1016/j.compgeo.2022.104696.
Xiao, H.B., Zhang, C.S., Wang, Y.H. and Fan, Z.H. (2011), "Pile-soil interaction in expansive soil foundation: Analytical solution and numerical simulation", *Int. J. Geomech.*, **11**(3), 159-166. https://doi.org/10.1061/(ASCE)GM.1943-5622.0000046.
Xiao, J., Yang, H., Zhang, J. and Tang, X. (2018), "Properties of drained shear strength of expansive soil considering low stresses and its influencing factors", *Int. J. Civ. Eng.*, **16**(10), 1389-1398. https://doi.org/10.1007/s40999-017-0268-6.
Yan, K. and Wu, L. (2009), "Swelling behavior of compacted expansive soils", In *Recent Advancement in Soil Behavior, in Situ Test Methods, Pile Foundations, and Tunneling*, 1-6. https://doi.org/10.1061/41044(351)1.

Ye, W., Zhang, Y., Chen, B., Zhou, X. and Xie, Q. (2010), "Shear strength of an unsaturated weakly expansive soil", *J. Rock Mech. Geotech. Eng.*, **2**(2), 155-161. https://doi.org/10.3724/SP.J.1235.2010.00155.

Zhan, T.L. and Ng, C.W. (2006), "Shear strength characteristics of an unsaturated expansive clay", *Can. Geotech. J.*, **43**(7), 751-763. https://doi.org/10.1139/t06-036.

Zhang, J., Niu, G., Li, X. and Sun, D. (2020), "Hydro-mechanical behavior of expansive soils with different dry densities over a wide suction range", *Acta Geotech.*, **15**, 265-278. https://doi.org/10.1007/s11440-019-00874-y.

Zhao, R., Wu, X., Zhu, G., Wang, X., Mei, A. and Zhang, X. (2022), "Experimental study on mechanical properties of highly swelling soft rocks in the Yanji Basin, Northern China", *Rock Mech. Rock Eng.*, **55**(3), 1125-1141. https://doi.org/10.1007/s00603-021-02754-y.

GC